UPDATE FOR PROPOSAL P12-06-119

Deeply Virtual Compton Scattering with CLAS at 11 GeV

A. Biselli, H. Egiyan, L. Elouadrhiri, D. Ireland, M. Holtrop, W. Kim, and F. Sabatié*

I. PHYSICS CONTEXT SUMMARY

A. Generalized Parton Distributions

Generalized Parton Distributions (GPDs) are physical observables which can provide deep insight about the internal structure of the nucleon. They contain the usual parton distribution functions (PDFs) and elastic form factors (FFs) as limiting cases or sum rules. In addition, GPDs allow to probe the nucleon as a 3-dimensional object, accessing for instance the quark orbital momentum and picturing the nucleon in quantum phase space.

Generalized Parton Distributions can be accessed through deep exclusive processes such as Deeply Virtual Compton Scattering (DVCS). Fifteen years ago, Mueller, Ji, Radyushkin and others [1–6] showed that the DVCS reaction $\gamma^* p \to \gamma p$ can, in the Bjorken limit, be factorized into a hard scattering kernel and a non-perturbative part, containing information about the electromagnetic structure of the nucleon in terms of four twist-2 chiral-even GPDs H, E, $\widetilde{H}$ and $\widetilde{E}$.

These GPDs depend on 4 variables $(x, \xi, t; Q^2)$. x characterizes the average light-cone momentum fraction of the struck quark in the loop (not directly accessible experimentally). ξ is the longitudinal momentum fraction of the transfer to the proton $\Delta = p - p'$ (where p and p' are the initial and recoil proton 4-vectors). Finally, $t = \Delta^2$ is the standard Mandelstam variable representing the momentum transfer between the virtual and real photons (or between the target and the recoil proton). The scale evolution of the GPDs (Q^2-dependence) has been worked out to next-to-leading order of α_S and beyond [7, 8].

B. Deeply Virtual Compton Scattering

The photon electroproduction $ep \to ep\gamma$ can either occur by radiation along one of the electron lines (Bethe-Heitler or BH) or by emission of a real photon by the nucleon (DVCS). The total amplitude $\mathcal{T}_{ep\gamma}$ is therefore the superposition of the BH and DVCS amplitudes:

$$|\mathcal{T}_{ep\gamma}|^2 = |\mathcal{T}_{\rm BH}|^2 + |\mathcal{T}_{\rm DVCS}|^2 + \mathcal{I}\,, \tag{1}$$

where $\mathcal{T}_{\rm DVCS}$ and $\mathcal{T}_{\rm BH}$ are the amplitudes for the DVCS and Bethe-Heitler processes, and $\mathcal{I}$ denotes the interference between these processes.

Using either a polarized beam or a longitudinally polarized target, two separate quantities can be extracted: the difference of cross section for opposite beam helicities or opposite target spin and the total cross section, which at leading twist can be written respectively as:

$$d\sigma^{\rightarrow} - d\sigma^{\leftarrow} \;=\; 2 \cdot \mathcal{T}_{BH} \cdot Im(\mathcal{T}_{DVCS})\,, \tag{2}$$

$$d\sigma^{\rightarrow} + d\sigma^{\leftarrow} \;=\; |T_{BH}|^2 + 2 \cdot \mathcal{T}_{BH} \cdot Re(\mathcal{T}_{DVCS}) + |T_{DVCS}|^2\,, \tag{3}$$

where the arrows correspond to the beam helicity. At low beam energy, the pure DVCS contribution is expected to be small with respect to the interference terms, which themselves are in general significantly smaller than the BH term. Note that the DVCS contribution to the difference of cross section only appears at higher twist. It is actually natural to express the DVCS amplitude $\mathcal{T}_{\rm DVCS}$ at leading twist more generally in terms of so-called Compton Form Factors (CFFs) which can be written at leading order as a function of the GPDs :

$$\mathcal{F} \;=\; \int_{-1}^{+1} dx\, F(x,\xi,t) \left(\frac{1}{\xi - x - i\epsilon} - \frac{1}{\xi + x - i\epsilon} \right) \qquad (F = H \text{ or } E) \tag{4}$$

$$\;=\; \mathcal{P} \int_{-1}^{+1} dx\, F(x,\xi,t) \left(\frac{1}{\xi - x} - \frac{1}{\xi + x} \right) + i\pi \Big(F(\xi,\xi,t) - F(-\xi,\xi,t) \Big) \tag{5}$$

The symbol $\mathcal{P}$ stands for Cauchy principal value. A CFF is complex-valued and we note Re CFF and Im CFF its real and imaginary parts. They are related by fixed-t dispersion relations [9–12], for example :

$$\mathrm{Re}\,\mathcal{H}(\xi,t) = 2\mathcal{P} \int_0^1 \frac{d\xi'}{\xi'} \frac{\mathrm{Im}\,\mathcal{H}(\xi',t)}{\frac{\xi^2}{\xi'^2} - 1} + \Delta(t) \tag{6}$$

where $\Delta(t)$ is a subtraction constant related to the D-term [13]. However the D-term is poorly known and most of DVCS measurements are made in the region $\xi' \leq 0.5$. Using

such a dispersion relations thus rely on models and may introduce biases in the extraction of GPDs from DVCS data. For that reason the real and imaginary parts of CFFs are taken as independent in some fitting procedures although they should obey the equality (6) from first principles.

II. EXTRACTION OF GENERALIZED PARTON DISTRIBUTIONS

by H. Moutarde (CEA Saclay, Irfu/SPhN), common with P12-06-114

A. Introduction

Extractions of GPDs is a much more demanding task than the extraction of Parton Distribution Functions (PDF) or Form Factors (FF) due to the complex functional structures of GPDs. Moreover, we need to extract four functions H, E, $\widetilde{H}$ and $\widetilde{E}$ of three variables (x, ξ, t) for each quark flavour (u, d and s). The Q^2-dependence is governed by the QCD evolution equations. Building a flexible yet robust GPD parametrization is very involved and the problem is still open today, but several groups have made attempts to fit GPDs (or CFFs) to data during the last few years. We will describe the different fitting methods in the following sections.

B. Local fits of CFFs

The first approach, pioneered in [14] and used in [15–18] assumes the independence of the real and imaginary parts of CFFs. The main assumptions are the validity of the twist-2 leading order analysis of existing DVCS measurements and a negligible contribution of $\mathrm{Im}\,\tilde{\mathcal{E}}$. Each kinematic bin (x_B, t, Q^2) is taken independently of the others, and the seven values $\mathrm{Re}\,\mathcal{H}$, $\mathrm{Im}\,\mathcal{H}$, $\mathrm{Re}\,\mathcal{E}$, $\mathrm{Im}\,\mathcal{E}$, $\mathrm{Re}\,\widetilde{\mathcal{H}}$, $\mathrm{Im}\,\widetilde{\mathcal{H}}$ and $\mathrm{Re}\,\widetilde{\mathcal{E}}$ are extracted simultaneously, so nothing prevents large fluctuations between two neighbouring kinematic bins. Moreover this method gives no clue on the extrapolation of the extracted CFF outside the data region. In the following we will refer to these fits as *local fits*. The model-dependence is almost as low as possible but the problem is often under-constrained.

C. Global fits of GPDs

In the spirit of the work done on PDFs and FFs, *global fits* require a physically motivated parametrization of GPDs and deal with all observables on all kinematic bins at once. The main advantage is obvious : the ability to extrapolate outside of the data region, and therefore evaluate for instance Ji's sum rule ($t \to 0$) or more generally, study the 3D partonic structure of the nucleon ($\xi \to 0$). The free coefficients entering the expressions for GPDs are determined either from PDFs and FFs or from DVCS data. Two such studies have been reported recently for DVCS [19, 20]. Note that fixed-t dispersion relations are used as a key ingredient in [19].

D. Hybrid fits of GPDs

The *hybrid* fitting procedure used in [15] is a combination of the previous two methods and has been applied with the main assumption of H-dominance and twist-2 accuracy. It involves a parametrization which fulfills the polynomiality condition of GPDs and includes Q^2 evolution at leading order in α_S. Since this function is otherwise arbitrary, its specific form is *a posteriori* validated by the quality of the fit. It makes it hazardous to extrapolate the extracted GPD outside the fitting domain as unphysical oscillations may occur. The model dependence is tested by a systematic comparison to local fits and an estimate of the systematic error induced by the H-dominance hypothesis. The good agreement of the local fits with respect to the global fits is a strong consistency check of this approach.

E. Neural network fits of GPDs

Neural network fits had been successfully performed for PDFs but their use for GPD extraction is quite recent. First results are described in [21] within the H-dominance assumption. Although it is too early to judge the advantages and shortcomings of this approach, it is worth noting that it is a new development in the field of GPD extraction.

III. CHANGES IN THE DETECTOR DESIGN

A. Calorimeter for photon detection

The proposed DVCS experiments at 11 GeV require an electromagnetic calorimeter for photon detection at forward angles. Such a calorimeter, called Inner Calorimeter (IC), has already been successfully used with CLAS in the 6 GeV era, and it can be used with CLAS12, as described in the original proposal. Another option that is currently being pursued is to use the electromagnetic calorimeter being designed and built for the CLAS12 forward tagging facility [22] instead of the IC. The CLAS12 Forward Tagger (FT) package consists of electromagnetic calorimeter, a scintillator hodoscope, and a tracking device located in front of the hodoscope, as illustrated in Fig. 1. This detector package will be provided by a group of European institutions: INFN, ORSAY, Saclay, and University of Glasgow. The design characteristics of FT calorimeter match very well with the requirements of the proposed DVCS experiments with the energy and position resolutions expected to be similar to that of IC. The new calorimeter will consist of approximately 400 crystals that have a rectangular shape with a cross section of 15×15 mm^2 and a length of 200 mm, corresponding to about 23 radiation lengths. The crystals will be arranged around the beamline to cover angles from 2° to 5° to contain the electromagnetic shower produced by electrons in the angular range from 2.5° to 4.5°. The crystals are placed inside a tungsten case to shield the forward part of CLAS12 from shower leakages. PbWO4 is the leading option for the forward tagger calorimeter modules due to its high resistant to radiation damage. Due to a presence of large magnetic field in the region of the calorimeter photodetectors based on semiconductors, such as Avalanche Photo Diode (APD) or Silicon Photo Multipliers (SiPM), are being considered for the readout.

B. Polarized target

A large part of the proposed experiment requires a longitudinally polarized ammonia target. The polarized target for CLAS12 is a collaborative effort involving multiple institutions: Jefferson Lab, University of Virginia, Christopher Newport University, and Old Dominion University. Funding for the polarized target R&D is provided by NSF through the Major Research Instrumentation Program. The target cryostat must house a horizontal, 1 K

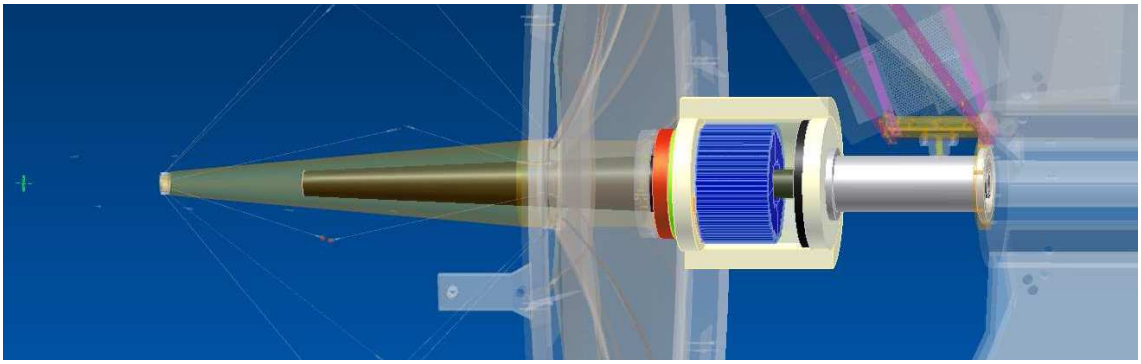

FIG. 1: CAD drawing showing the integration of the Forward Tagger into CLAS12. The new calorimeter shown in blue is located at about 190 cm from the interaction point, shown by the green cross, and is enclosed in a Rohacell case to provide thermal insulation. The scintillation counter (green) and first tracker layer (red) are located in front of the calorimeter. A tungsten cone in black shields the calorimeter and the scintillator hodoscope from Møller electrons and electromagnetic background created by the beam.

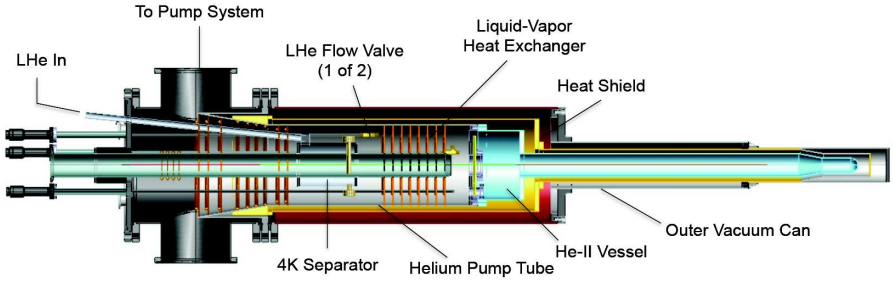

FIG. 2: A schematic view of the polarized solid target cryostat and the target insert for CLAS12.

helium evaporation refrigerator, the sample insert, and additional instrumentation for the microwave and NMR operations. The cryostat will be designed to operate in a warm bore magnetic field, and in this manner will resemble the existing Hall B Frozen Spin Target [23], with the evaporation refrigerator replacing the latter target's ^{3}He/^{4}He dilution refrigerator. A conceptual design is shown in Figure 2. This updated design differs from that shown in the original proposal.

The original design was modeled upon refrigerators built more than 40 years ago for the earliest polarized targets at Saclay. These were characterized by loading the target sample into a small cup that was continuously filled with superfluid helium. Because of

the small volume of the cup, this design is sensitive to small variations in either beam heating or delivery of helium coolant to the cup. The current design is based closely on the vertical evaporation refrigerators employed in the existing Hall B and Hall C polarized targets [24, 25]. Here the target sample is suspended into a much larger bath of superfluid helium (about 1 liter) which ensures greater stability during heating and cooling transients. For this horizontal refrigerator, a stainless steel "dam" will confine the superfluid to the evaporation chamber located in the downstream end of the target cryostat. A polyimide cold seal, similar to one developed for the Frozen Spin Target, will be employed to seal the target sample inside this volume.

In all other respects the evaporation refrigerator is identical to the one described in the original proposal. Liquid helium is supplied to the refrigerator though a transfer line from a dewar located outside the detector. The liquid first enters a separator pot which will have a "donut"-like shape in order not to obstruct the beam bath. In this pot liquid helium is separated from the vapor using a thin sintered filter. The vapor is pumped away, cooling a heat shield that surrounds the downstream portion of the cryostat. Liquid from the separator is delivered to the evaporation chamber through a fine needle valve and is cooled close to 1 K by a heat exchanger between the 4 K liquid and the cold vapor pumped from the evaporation chamber by a series of pumps located outside the detector. The microwave radiation needed to polarize the sample will be introduced through a dedicated waveguide extending into the evaporation chamber. This guide will have a slit directly underneath the sample, providing continuous microwave radiation to the sample material. The sample will consist of fine ($1 - 2$ mm) irregular beads of frozen ammonia loaded into a small PCTFE cup with aluminum entrance and exit windows. A NMR coil will be wrapped around the cup to determine the target polarization.

C. Forward vertex tracker

The use of a Forward Vertex Tracker, currently designed as 3 double-layer Micromegas planes around the beamline, in combination with the Drift Chambers will improve the CLAS12 tracking performance. This FVT will be located 30 cm downstream of the target, and will therefore dramatically enhance the vertex resolution. For single particles, the vertex resolution along the beam axis will be improved by a factor of 3, while an order of magnitude

is expected on the impact parameter. Besides, the electron azimuthal angle resolution at high momentum will be increased by roughly 50%, while keeping the polar angle and momentum resolutions basically unchanged.

IV. EXPERIMENTAL STATUS

Experiments E00-110, E03-106 in Hall A [26, 27] and E01-113a in Hall B [28] ran in 2004-2005 and since PAC30, published DVCS cross sections and asymmetries, used by various groups to extract CFFs or GPDs as described in the previous section. More data from experiments E07-007 in Hall A and E01-113b, E05-114 in Hall B are currently being analyzed. Finally, the transverse target DVCS experiment E08-021 in Hall B is planned for 2012. Overall, the Jefferson Lab data set at 6 GeV is so far the largest data set on DVCS in the world in the valence quark region. The main limitation is of course the relatively low beam energy which forced rather low-Q^2 values and for some observables, the integrated luminosity. In order to unravel the complete GPD information from data, it is important to have accurate measurement of all types of observables in as large a kinematical domain as experimentally accessible and it is therefore essential to extend these measurements at higher energy with CLAS12.

V. SUMMARY OF P12-06-119 REQUEST

We maintain the requested **80 days of beam time to measure beam spin asymmetries with the liquid hydrogen target and 120 days of beam to measure target spin asymmetries using the longitudinally polarized target**. The expected statistical accuracy for the $\sin\phi$ moment of the measured asymmetries ranges from 1% at low-x_B and low-Q^2 to about 10% at high-x_B and high-Q^2, with systematic errors of around 5% in the unpolarized target case and 7% in the longitudinally polarized target case, which match the average statistical error of the data in the full kinematical range.

These data will constitute an unprecedented data set, both in precision and in kinematical coverage, allowing for a dramatic improvement in GPD extraction as shown on Fig. 3, where the CFF $\mathcal{H}$ extracted from the 6 GeV JLab data is compared to what can be achieved with CLAS12 pseudo-data expected in this proposal.

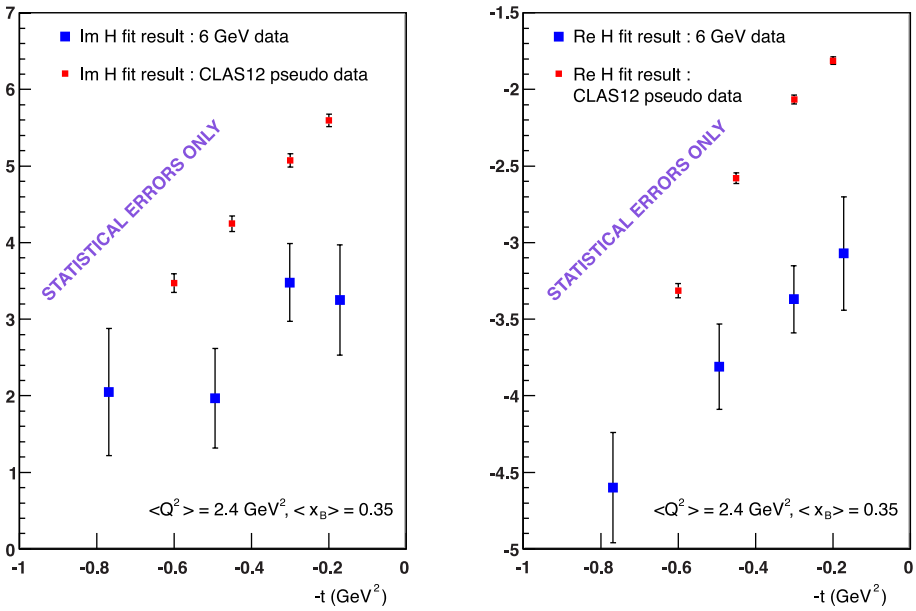

FIG. 3: Imaginary part (left) and real part (right) of CFF $\mathcal{H}(t)$ extracted by H. Moutarde [15] for existing JLab 6 GeV data (blue squares) and with CLAS12 pseudo-data (red squares).

VI. SUMMARY

The first extractions of GPDs or CFFs from early Jefferson Lab and HERMES DVCS data are very encouraging, and a lot of progress has been made by the different groups involved in the analyses. The abundance of 11 GeV data will allow for more flexible functional forms to be fitted, which will help to relax the drastic hypotheses made so far such as H-dominance, twist-2 dominance, and leading order analysis. There is no doubt that in the coming years phenomenologists will refine their fitting techniques and will be ready to analyze a large quantity of data from the Jefferson Lab upgrade.

There have been modifications to the detector package since the submission of the original proposal. The exact effects of these modifications are currently being studied, but these changes are expected to have a small impact on the proposed experiments. The new data from proposed experiments with its large kinematic coverage, along with accurate cross section measurements from Hall A and other experiments, will greatly contribute towards

the improvement of our knowledge of the 3D partonic nucleon structure.

---

[1] D. Mueller *et al.*, Fortschr. Phys. **42**, 101 (1994).

[2] X.-D. Ji, Phys. Rev. **D55**, 7114 (1997).

[3] X.-D. Ji, Phys. Rev. Lett. **78**, 610 (1997).

[4] X.-D. Ji, W. Melnitchouk, and X. Song, Phys. Rev. **D56**, 5511 (1997).

[5] A. V. Radyushkin, Phys. Lett. **B380**, 417 (1996).

[6] A. V. Radyushkin, Phys. Rev. **D56**, 5524 (1997).

[7] D. Mueller, Phys. Lett. **B634**, 227 (2006).

[8] K. Kumericki, D. Mueller, K. Passek-Kumericki, and A. Schafer, Phys. Lett. **B648**, 186 (2007).

[9] O. Teryaev, hep-ph/0510031 (2005).

[10] I. Anikin and O. Teryaev, Fizika **B17**, 151 (2008).

[11] I. Anikin and O. Teryaev, Phys.Rev. **D76**, 056007 (2007).

[12] M. Diehl and D. Ivanov, Eur.Phys.J. **C52**, 919 (2007).

[13] M. V. Polyakov and C. Weiss, Phys.Rev. **D60**, 114017 (1999).

[14] M. Guidal, Eur. Phys. J. **A37**, 319 (2008).

[15] H. Moutarde, Phys. Rev. D **79**, 094021 (2009).

[16] M. Guidal and H. Moutarde, Eur.Phys.J. **A42**, 71 (2009).

[17] M. Guidal, Phys.Lett. **B689**, 156 (2010).

[18] M. Guidal, Phys. Lett. **B693**, 17 (2010).

[19] K. Kumericki and D. Mueller, Nucl. Phys. **B841**, 1 (2010).

[20] G. R. Goldstein, J. G. Hernandez, and S. Liuti, (2010), * Temporary entry *.

[21] K. Kumericki, D. Mueller, and A. Schafer, (2011), * Temporary entry *.

[22] M. Battaglieri *et al.*, JLab Experiment E12-11-005 (2011).

[23] C. D. Keith, AIP Conf. Proc. **1149**, 886 (2009).

[24] C. D. Keith *et al.*, Nucl. Instrum. Meth. **A501**, 327 (2003).

[25] T. D. Averett *et al.*, Nucl. Instrum. Meth. **A427**, 440 (1999).

[26] C. Munoz Camacho *et al.*, Phys. Rev. Lett. **97**, 262002 (2006).

[27] M. Mazouz *et al.*, Phys. Rev. Lett. **99**, 242501 (2007).

[28] F. X. Girod *et al.*, Phys. Rev. Lett. **100**, 162002 (2008).